ACS APPLIED POLYMER MATERIALS

pubs.acs.org/acsapm Article

Survey of Conductive Polymers for the Fabrication of Conformation Switching Nucleic Acid-Based Electrochemical Biosensors

Alexander Shaver, Kyle Mallires, Jonathan Harris, Jonathan Kavner, Bo Wang, Rebecca Gottlieb, Juan Lión-Villar, María Ángeles Herranz, Nazario Martín, and Netzahualcóyotl Arroyo-Currás*

Cite This: ACS Appl. Polym. Mater. 2024, 6, 541−551 Read Online

ACCESS | Metrics & More | Article Recommendations | Supporting Information

ABSTRACT: Electrochemical biosensors are a continuously evolving technology with great potential for applications in human health. With the continuous glucose monitor as an example, these sensors are capable of accurately determining molecular concentrations directly in the human body. A specific class of biosensors, termed conformation switching nucleic acid-based electrochemical sensors (NBEs), relies on the affinity of oligonucleotides for molecular recognition and their conformational dynamics upon target binding for signal generation. Currently, most NBEs are fabricated via the self-assembly of alkylthiol monolayers on Au electrodes. However, this architecture is limited in terms of stability and the breadth of supporting materials with which it is compatible. Here, to explore alternative material options for the fabrication of NBE sensors, we form conductive polymers of aromatic amines, thiophenes, and pyrroles on platinum electrodes. Altering many parameters throughout the study, we determine the extent to which the polymers passivate the electrode surface and then couple redox reporters or reporter-modified nucleic acids. We discuss the limitations and benefits of each polymer for the formation of NBE sensors and provide future directions to continue the quest for alternative sensor materials.

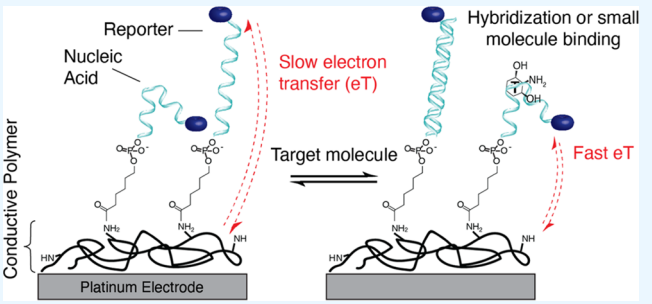

KEYWORDS: *conductive polymers, electrochemical sensor, nucleic acids, redox reporter, thiophene*

INTRODUCTION

Electrochemical biosensors are a class of technology with great value to human health and great promise for wide-ranging future applications. As a case in point, the continuous glucose monitor has undoubtedly improved both the life expectancy and quality of life for individuals with Type I diabetes.[1] Beyond this well-known, commercialized example, electrochemical biosensors are being developed for biomedical applications, including cancer cell detection,[2] biomarker tracking,[3] blood alcohol analysis,[4] and therapeutic drug monitoring.[5,6] Thanks to their desirable functional properties like low cost,[7,8] compatibility with biological fluids,[9,10] and inherent analytical capabilities, electrochemical biosensors are ideal candidates for clinical translation. As examples of potential future uses, these sensors could be interfaced with wound dressings to monitor inflammation and infection.[11] They could be grafted to biomedical implants or prosthetics to track healing.[12,13] They could even be deposited on contact lenses for the detection of ocular diseases.[14] However, each of these applications may require different supporting materials for the proper function and compatibility with the associated surface. Therefore, there is a continuing need for the development of biosensor materials.

Of course, not all potential analytes for electrochemical biosensors can be detected using enzymatic reactivity, as with glucose and glucose oxidase. Instead, a more generalizable approach is affinity biosensors, which can be developed for nearly any molecule of interest, regardless of enzymatic or electrochemical reactivity. A specific type of affinity biosensor, conformation switching nucleic acid-based electrochemical sensors (NBEs), are particularly well suited for continuous molecular measurements because they are reversible and do not require the addition of exogenous reagents.[3,9] With these attributes in mind, NBEs have the potential to be developed as clinically relevant molecular monitors for the management and treatment of human health. NBEs rely on nucleic acid dynamics upon target binding to generate sensor signaling. In general, the nucleic acids are immobilized onto an electrode surface via a functionality (e.g., alkanethiol for attachment to gold or amine for coupling to carboxylic acid) on one end. The other end is covalently modified with a redox reporter—typically methylene blue (MB)—that, upon target binding to the nucleic acids, changes its rate of electron transfer (Figure

Received: September 16, 2023
Revised: December 13, 2023
Accepted: December 18, 2023
Published: December 28, 2023

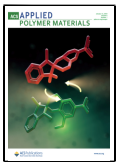

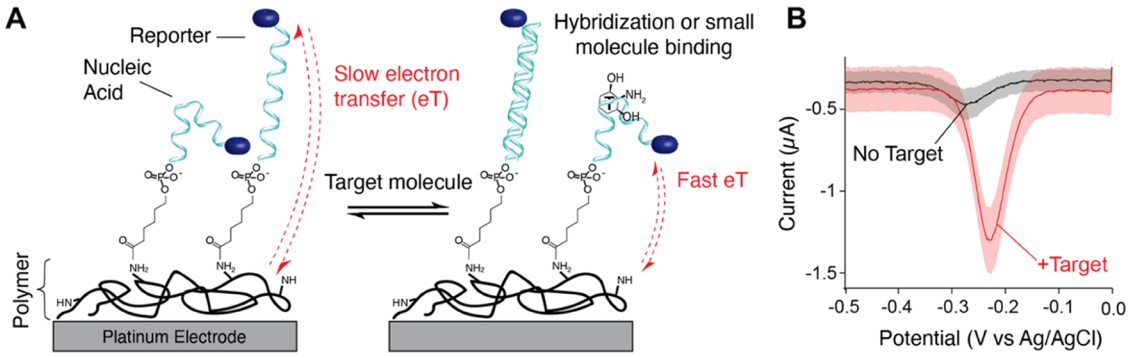

Figure 1. Proposed NBE sensor anatomy and signaling. (A) We used platinum electrodes as a model system for this study and evaluated the feasibility of fabricating NBEs via coupling of redox reporter-modified nucleic acid aptamers to electropolymerized conductive polymers. Target binding to the aptamers should induce a conformational change that alters the electron transfer kinetics of the reporter. Here illustrated for the case of small molecule-binding to the aptamers, which should ideally result in increased electron transfer. (B) When interrogated via square-wave voltammetry (SWV), changes in the target concentration should theoretically be seen as a change in the peak current or area under the voltammogram.

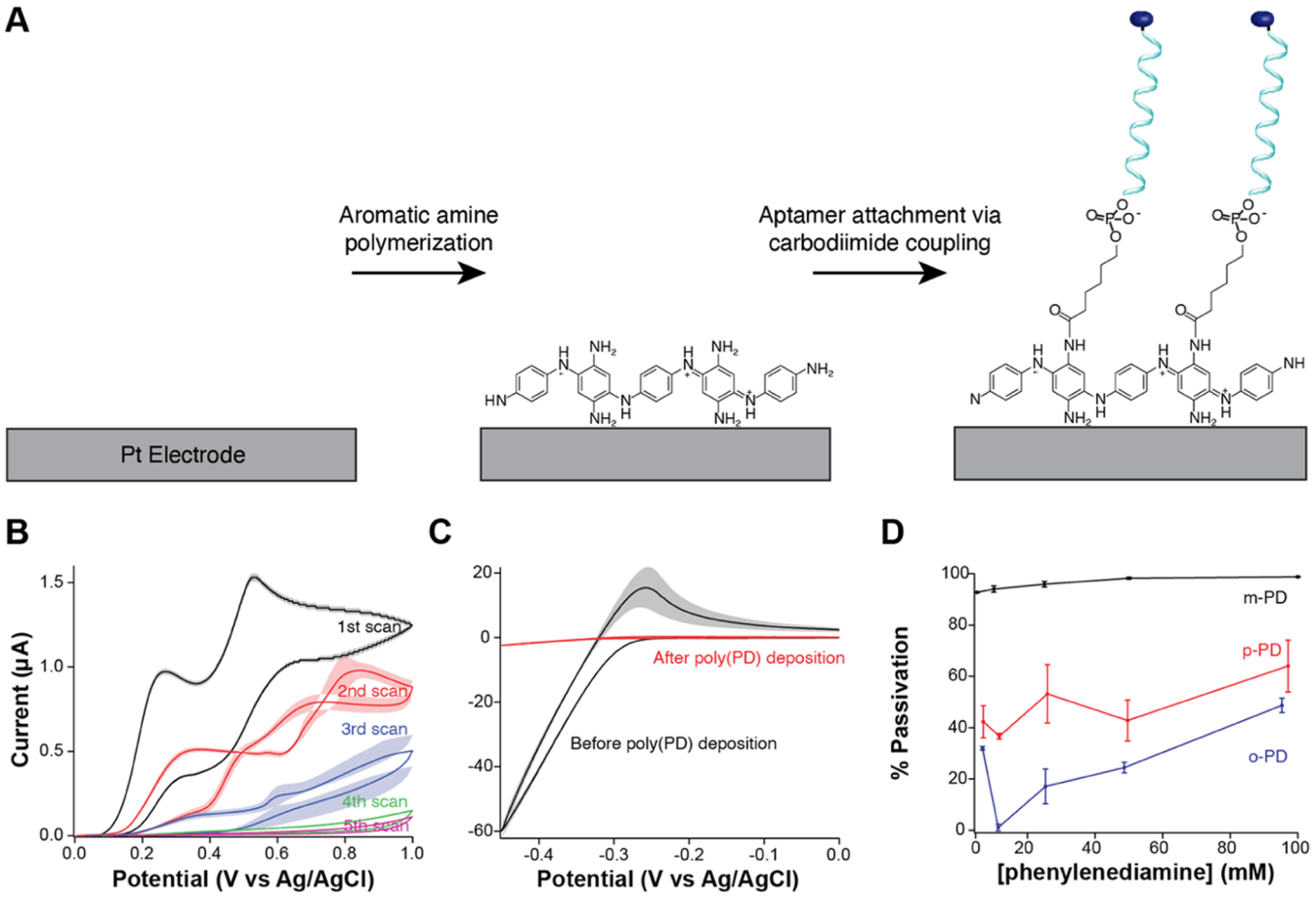

Figure 2. Platinum electrode passivation with polymers of aromatic amines. (A) We fabricate NBE sensors on Pt electrodes following a two-step procedure: first, we deposit a conductive polymer via electropolymerization from a monomer solution, and second, we couple the reporter methylene blue MB- to carboxylic acid-modified oligonucleotides via carbodiimide chemistry. (B) poly(PD) films were formed by repeated CV scanning in monomer solution. The representative traces shown here polymerized 25 mM *p*-PD at a scan rate of 50 mV s^{-1}. (C) Recording CV (1 V s^{-1}) in 50 mM sulfuric acid before and after polymer deposition reveals a significant passivation of the oxygen reduction reaction (ORR). The representative traces shown here polymerized 25 mM *m*-PD at a scan rate of 50 mV s^{-1}. (D) By extracting the current at −0.45 V in the sulfuric acid CVs and calculating percent passivation, as shown in eq 1, we can determine the relative surface passivation for different isomers and concentrations of PD monomers. Solid lines are the mean, and shaded areas and error bars represent the standard deviation calculated from 8 electrodes.

1A).[10,15] The change in reporter electron transfer can be detected via a variety of electrochemical techniques, most commonly square-wave voltammetry (SWV), in which monotonic increases or decreases in the peak height or area under the curve occur with changing target concentration (Figure 1B).[16]

https://doi.org/10.1021/acsapm.3c02206
ACS Appl. Polym. Mater. 2024, 6, 541−551

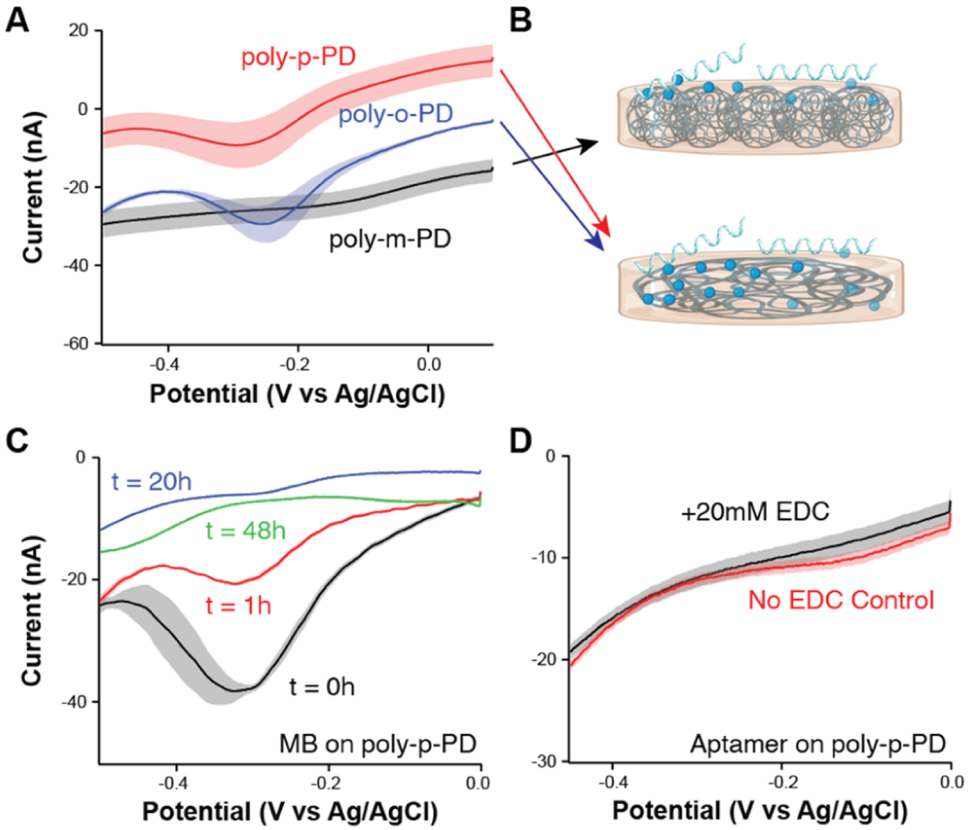

Figure 3. Redox signaling capability of poly(PD) films. (A) By holding all other polymerization parameters the same (50 mM [monomer]; 100 mV s^{-1} scan rate), we reveal that poly(*m*-PD) films do not allow electron transfer to attached MB, unlike films of poly(*p*-PD) or poly(*o*-PD). (B) Schematic representations of (top) poly(*m*-PD) or (bottom) poly(*p*-PD)/poly(*o*-PD) film density. (C) By interrogating poly(*p*-PD) and MB-ester modified electrodes every 12 s, we demonstrate that reporter signaling is lost within 2 days. (D) Coupling MB- and carboxylic acid-modified oligonucleotides to poly(*p*-PD) films instead of MB-ester, we can no longer resolve faradic current from MB reporters. poly(*p*-PD) films for panels (C, D) were formed from 25 mM solutions of *p*-PD at 50 mV s^{-1}. SWV was performed with an amplitude of 25 mV and a frequency of 60 Hz. Shaded areas represent the standard deviation calculated from 8 electrodes.

NBE sensors have been deployed for continuous molecular monitoring in the veins,[17] brains,[18] and interstitial fluid[19,20] of rodents. However, all of these demonstrations have employed the same chemistry for immobilization of nucleic acids: alkanethiol monolayers on gold. While powerful in terms of rapid, simple fabrication, thiols on gold suffer several limitations, including poor stability in biological fluids[21] and rapid accumulation of nonspecifically bound proteins.[22,23] Moreover, gold itself may not be compatible with every potential NBE sensor application. In this work, we seek to expand the library of materials for the fabrication of NBEs by investigating the formation and modification of conductive polymers. Conductive polymers are a class of materials that have been widely studied for their electrical, mechanical, and optical properties.[24−26] They have been deployed in many biomedical applications, from tissue engineering to wound healing to drug delivery.[24] Additionally, they are known to have outstanding biocompatibility and can be easily fabricated and modified.[25]

Here, we survey conductive polymers of thiophenes, pyrroles, and aromatic amines, specifically evaluating their compatibility with NBE sensing. We note that additional classes of polymers may have desirable characteristics for sensing but focus on these three as a starting point. By electropolymerizing films on Pt electrodes and then coupling redox reporters or reporter-modified nucleic acids, we discover the benefits and limitations of several polymer options as they relate to the fabrication of NBE sensors. While no studied option enabled creation of a functional NBE sensor, our demonstration of electrode functionalization and discussion of polymer behaviors provide a platform for further exploration of combining the promise of NBEs with the chemical structure versatility of conductive polymers.

RESULTS AND DISCUSSION

For the attempted creation of NBE sensors on conductive polymers and to accurately determine differences in voltammetric current arising from the polymers themselves versus redox reporters, we follow a two-step electrode functionalization process where initially formed polymers are subsequently coupled to redox reporters or reporter-modified nucleic acids (Figure 2A). In this work, all polymers were formed on polycrystalline Pt electrodes, and all measurements reported are based on a three-electrode cell configuration, using a Pt counter electrode, an Ag|AgCl reference electrode, and Pt microelectrode arrays as the working electrode (see the Materials and MethodsSection). Unless otherwise noted, all experiments were conducted in phosphate-buffered saline (PBS). All measurements represent the average and standard deviation across 8 electrode array elements, interrogated simultaneously via a multichannel potentiostat. Additional details are provided in the Materials and Methods Section.

https://doi.org/10.1021/acsapm.3c02206
ACS Appl. Polym. Mater. 2024, 6, 541−551

Conductive Polymers of Aromatic Amines. As a first venture into using conductive polymers as the supporting material for NBE sensors, we electrochemically formed polymers of aromatic amines (Figure 2A). Specifically, we electropolymerized films of polyphenylenediamine, poly(PD), by cyclic voltammetry (CV) in monomer solutions of three different PD isomers: *ortho*-PD (*o*-PD), *meta*-PD (*m*-PD), and *para*-PD (*p*-PD). By cycling in PBS with 5 mM sodium sulfate as the counterion, we reveal progressively less current with each cycle (Figure 2B). We note that a mechanistic discussion of the various redox processes observed in the voltammograms of Figure 2B is outside the scope of this work. However, prior published work[27] provides a detailed discussion using voltammetry and mass spectrometry. The loss of current indicates surface passivation via successful deposition of polymer film on the Pt electrode surface. Passivation is important to prevent current from unwanted reactions on the electrode, especially the oxygen reduction reaction (ORR) that overlaps with the reduction of the benchmark redox reporter MB.[22] ORR passivation can also be visualized by CV interrogation in dilute (50 mM) sulfuric acid (Figure 2C). Before poly(PD) deposition, there is a large current at voltages more negative than −0.3 V corresponding to the ORR (Figure 2C, black trace). After poly(PD) deposition, however, that current is greatly diminished due to coverage of the Pt surface with the formed poly(PD) films (Figure 2C, red trace). By extracting the current at −0.45 V for each of these traces and using eq 1

$$\% \text{ passivation} = \frac{i_{\text{before}} - i_{\text{after}}}{i_{\text{before}}} \quad (1)$$

we present a measure of percent passivation of the electrode surface. By forming poly(PD) films from five different monomer concentrations (5, 10, 25, 50, and 100 mM) for all three PD isomers, we were able to determine that *m*-PD passivates electrodes the most, with ∼90% passivation for all monomer concentrations used (Figure 2D, black trace). *p*-PD and *o*-PD, on the other hand, range from ∼0 to 60% passivation depending on concentration, with *p*-PD always passivating the surface to a larger extent than *o*-PD (Figure 2D, red vs blue trace). This method of determining percent surface passivation is also used in experiments below with alternative polymer chemistries.

Following polymer formation, we can couple redox reporters or reporter-modified nucleic acids to impart a signaling capability to the electrodes. For rapid prototyping during initial experiments, we chemically coupled a methylene blue (MB) *N*-hydroxysuccinimide (NHS) ester (MB-ester, 100 μM) that reacts spontaneously with primary and secondary amines on the polymer films. Interrogating the resultant surfaces via SWV, we observe a faradic peak from the attached MB (Figure 3A). The magnitude of this peak compared to the baseline current demonstrates the high signal-to-noise ratio (SNR) in our voltammograms. High SNR is indicative of good passivation while retaining the conductivity necessary for electron transfer to the attached redox reporters. By using this measure of SNR, we were able to optimize both the monomer concentration and CV scan rate used during polymerization (Figure S1). Specifically investigating *p*-PD as an example, we show that any monomer concentration <100 mM during poly(*p*-PD) formation enables signal resolution of attached MB under SWV (Figure S1A). Similarly, any CV scan rate >5 mV s^{-1} employed during polymerization enables good signal resolution (Figure S1B). As such, parameters in these ranges were used in poly(PD) experiments moving forward. Using specifically a scan rate of 50 mV s^{-1} to polymerize *p*-PD, we also recorded depth images with a laser microscope (thin film profilometry) to estimate the thickness of PD films (Figure S2). These images reveal poly(*p*-PD) thicknesses from 13−25 nm, depending on the number of CV scans.

Beyond optimization of polymerization parameters, we next sought to determine the best PD isomer for sensor fabrication. By creating films from all three isomers using identical parameters and then subsequently coupling the MB-ester, we discovered that unlike poly(*p*-PD) and poly(*o*-PD), films of poly(*m*-PD) do not allow electron transfer to reporters (Figure 3A). Combined with the fact that poly(*m*-PD) gave significantly higher levels of electrode passivation than the other two films (Figure 2D), we believe this result indicates that polymers formed from *m*-PD are denser, thereby restricting MB to the surface of the thick polymer (Figure 3B). Previous work has also commented on the balance of polymer thickness and charge transfer permeability for polymers of aromatic amines.[28] Because of this limitation, we moved forward with *p*-PD as our isomer of choice, as it gave greater passivation than *o*-PD while still allowing electron transfer to/from reporters.

Creating polymers from 25 mM solutions of *p*-PD at a scan rate of 50 mV s^{-1}, we also sought to determine the signal stability of the polymer-coupled MB reporters. In the field of NBE sensors, signal stability over time remains a major issue,[29] so we wanted to determine if poly(*p*-PD) films could compete with existing technologies. By interrogating these MB-modified polymers every 12 s by SWV, we found that signal is lost within 48 h (Figure 3C), a lifetime shorter than many thiol-on-gold strategies.[22] Finally, we wanted to see if a sensor signal could be generated from polymer-attached nucleic acids. Following polymerization of *p*-PD, we coupled MB- and carboxylic acid-modified aptamers via overnight incubation in 1 μM DNA and 20 mM carbodiimide reagent (EDC). This procedure enables cross-linking between free amines on the polymer surface and the carboxylic acid groups on the 5′ end of the aptamers. Interrogating the resulting surfaces via SWV, we observed no faradic peak from aptamer-attached MB (Figure 3D).

Since we have previously demonstrated that EDC coupling reactions work well in our hands, we believe this lack of signal is not indicative of a failure to couple but rather of a property of the polymer that prevents electron transfer to the aptamer-attached reporters. Specifically, we hypothesize that the poly(*p*-PD) films may be so thick that aptamers attached to the surface are too far away from the electrode to undergo electron transfer. Moreover, unlike MB-ester, which is small enough to penetrate poly(*p*-PD) or poly(*o*-PD) films to a depth that enables electron transfer, the much larger nucleic acids are restricted to the polymer surface, much the same as MB-ester is with the denser/more passivating poly(*m*-PD) films. As such, we are unable to resolve current from aptamer-attached reporters and, thereby, are unable to generate NBE sensor signaling using poly(PD) films on Pt electrodes.

Conductive Polymers of Thiophenes and Pyrroles. To circumvent the density/thickness limitations of poly(PD) films, we alternatively modified Pt electrodes with thiophene- and pyrrole-based polymers. These polymers have been widely used in the field of electrochemistry,[28,30,31] and they are known to grow linearly from the electrode surface, thereby preventing

https://doi.org/10.1021/acsapm.3c02206
ACS Appl. Polym. Mater. 2024, 6, 541−551

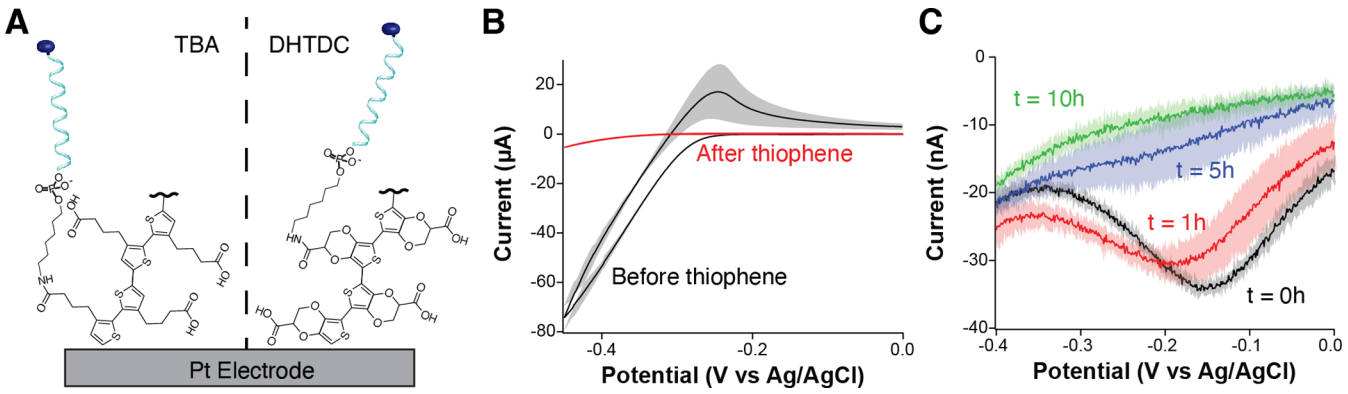

Figure 4. Platinum electrode passivation with thiophene polymers. (A) We electrodeposited polymers of both TBA (left) and DHTDC (right). (B) Typical CVs (1 V s^{-1}) in 50 mM sulfuric acid before and after polymer deposition reveal a significant passivation of the ORR. (C) Without further modification by redox reporters, SWVs (25 mV, 250 Hz) recorded every 10 min on TBA-functionalized surfaces reveal a progressive loss of conductivity that precludes interrogation at negative potentials. Solid lines are the mean and, shaded areas, the standard deviation calculated from 8 electrodes.

Table 1. Polymerization Parameters and the Extent of Electrode Passivation

monomer	solvent/counterion	EC method/parameters	% passivation
5−100 mM *m*-PD	PBS/5 mM Na_2SO_4	CV, 0 to 1 V, 100 mV s^{-1}	93−99
5−100 mM *o*-PD	PBS/5 mM Na_2SO_4	CV, 0 to 1 V, 100 mV s^{-1}	0−44
5−100 mM *p*-PD	PBS/5 mM Na_2SO_4	CV, 0 to 1−1.5 V, 5−100 mV s^{-1}	30−69
10 mM TBA	acetonitrile/100 mM TBATFB	CA, 1.35 V for 20 s	63−70
10 mM DHTDC	acetonitrile/100 mM TBATFB	CA, 1.35 V for 20 s	40−64
10 mM DHTDC	acetonitrile/100 mM TBATFB	CA, 1.1 V for 60 min	93−98
10 mM DHTDC	water/100 mM VBS	CA, 0.9 V for 60 min	93−94
10 mM TEA	acetonitrile/100 mM TBATFB	CA, 1.4 V for 60 min	52−84
10 mM MTEA	acetonitrile/100 mM TBATFB	CA, 1.4 V for 60 min	87−95
50 mM PPA	saline	30 × [1 V for 1 s → 0 V for 10 s]	63−64

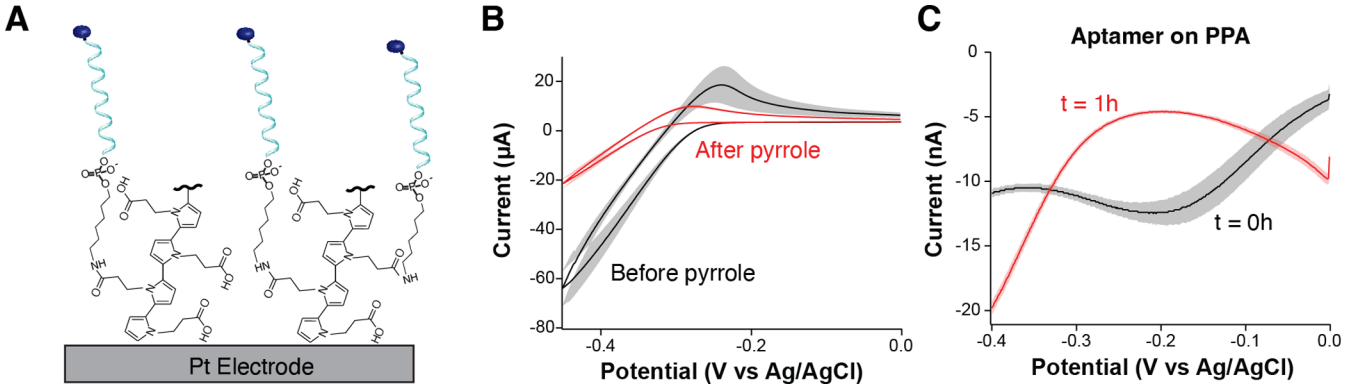

Figure 5. Platinum electrode passivation using pyrrole polymers. (A) We formed polymers of 1*H*-pyyrole propionic acid (PPA). (B) Recording CV (1 V s^{-1}) in 50 mM sulfuric acid before and after polymer deposition reveals a significant passivation of the ORR. (C) Recording SWVs (25 mV, 60 Hz) every 10 s reveals a rapid (<1 h) loss of conductivity like that seen with thiophene polymers. Solid lines represent the mean and, shaded areas, the standard deviation calculated from 8 electrodes.

the dense cross-linking seen with poly(PD) films. By using monomers with either a free amine or carboxylic acid side chain, we were able to make use of carbodiimide coupling for downstream tethering of functional groups (Figure 4A). To create initial thiophene-based polymers, we incubated Pt electrodes in 10 mM solutions of either thienyl butyric acid (TBA) or 2,3-dihydrothieno[3,4-B][1,4]dioxine-2-carboxylic acid (DHTDC) with 100 mM tetrabutylammonium tetrafluoroborate (TBATFB) in acetonitrile and interrogated them via chronoamperometry (CA). For these experiments, the potential was held at 1.35 V for 20 s to cause polymerization, as previously reported.[32] After verifying polymer deposition on the surface via passivation of the ORR (Figure 4B), we investigated how the polymers changed over time under voltammetric interrogation. By running SWV (25 mV, 250 Hz) every 10 min for 24 h on TBA-functionalized electrodes, we noticed that within 5−10 h, the polymers lost conductivity (Figure 4C). Unfortunately, this result indicates that we cannot interrogate MB on thiophene-based polymers, as the negative potentials needed to reduce MB will also passivate the surface and prevent electron transfer.

https://doi.org/10.1021/acsapm.3c02206
ACS Appl. Polym. Mater. 2024, 6, 541−551

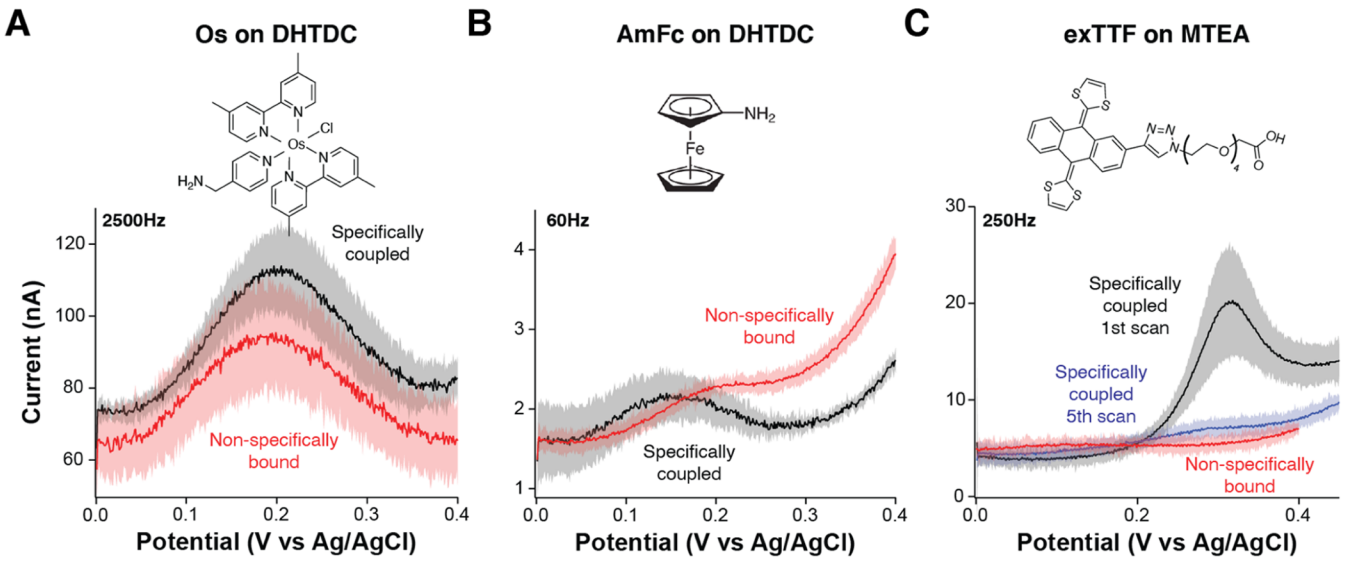

Figure 6. Alternative redox reporters on thiophene polymers. To avoid the loss of conductivity seen at negative voltages with thiophene-based polymers, we coupled three different redox reporters that undergo oxidation at potentials higher than 0 V vs AglAgCl. (A) Coupling of an Os-based complex previously reported by Pellitero et al.[35] to films of DHTDC (polymerized at 1.35 V for 20 s) gives well-defined faradic peaks. Unfortunately, we observed a large extent of irreversible, nonspecific complex binding to the surface. (B) Coupling AmFc to films of DHTDC (polymerized at 1.1 V for 60 min) displays less nonspecific binding but suffers from poor stability in chloride-containing media. (C) Coupling a π-extended tetrathiafulvalene (exTTF) molecule previously reported by Li et al.[37] to films of MTEA (polymerized at 1.4 V for 60 min) displays excellent coupling with no nonspecific binding. However, the fabricated surfaces lose a signal within five SWV scans. All polymers were formed from a 10 mM monomer solution with 100 mM TBATFB in acetonitrile. The displayed SWV (25 mV) was performed in PBS at the frequency indicated. Solid lines are the mean, and shaded areas represent the standard deviation calculated from 8 electrodes. Chemical structures for the Os complex and exTTF were reproduced from refs 35 and, 37 respectively, with permission from the Royal Society of Chemistry.

To ensure that the above self-passivation was not an artifact of the polymerization parameters, we investigated other monomers, counterions, solvents, CA potentials, and times for polymerization (Table 1). To optimize the potentials held during electropolymerization, we recorded CVs in monomer solutions and determined the onset potentials for oxidation (Figure S3A). By holding the potential just above the oxidation onset for 60 min (rather than 20 s at higher potentials as above), it is thought that polymerization of the monomer is slower, and more uniform polymers form on the electrodes. Additionally, the potential held during polymerization is known to play a role in the conductivity of the resulting polymer.[33] Following this logic, we formed polymers of DHTDC in two ways: (1) by holding the electrodes at 1.1 V in acetonitrile with 100 mM TBATFB; and (2) by holding them at 0.9 V in water with 100 mM sodium vinylbenzenesulfonate (VBS) as the counterion/copolymer. By monitoring the passivation of the ORR, we determined that this method of lower potential for a longer time does, in fact, increase passivation of the surface compared to the previous parameters (Table 1). However, this increased passivation does not provide benefits for signal resolution of surface-attached reporters. We followed each condition with overnight coupling to 100 μM new methylene blue (NMB; a derivative of MB with an available amine for coupling) in the presence of 20 mM EDC. However, no combination of parameters tested enabled SWV (25 mV, 60 Hz) signal from NMB reporters (Figure S3B). Therefore, we believe the issues of thiophene polymer conductivity when interrogated at negative potentials are not a result of polymerization parameters but rather an inherent limitation of the polymer chemistry.

As mentioned above, we also tried a pyrrole-based polymer for the formation of sensing layers on the Pt electrodes. Specifically, we polymerized 1*H*-pyrrole propionic acid (PPA) via repeated potential pulsing in 50 mM monomer solutions in saline (Figure 5A). Following a previously reported method,[34] for 30 repetitions, we jumped the potential to 1 V for 1 s to initiate polymerization and then let the electrodes rest at 0 V for 10 s to replenish PPA monomers at the surface. After verifying polymer deposition on the surface via passivation of the ORR (Figure 5B), we coupled MB- and amine-modified aptamers (1 μM) to the polymer with EDC. Unfortunately, running SWV (25 mV, 60 Hz) every 10 s again revealed no resolvable signal from aptamer-attached MB, in addition to a rapid alteration in the background current (Figure 5C). These results indicate that, like thiophenes, pyrrole-based polymers cannot be used for interrogation at negative potentials.

Reporters with Positive Redox Potentials. To overcome the limitation imposed at negative potentials by thiophene- and pyrrole-based films, we investigated the attachment of several reporters that have redox potentials above 0 V. These coupling reactions were carried out after polymer deposition via incubation with 100 μM redox reporter in 250 mM NaCl and 5 mM $MgCl_2$. Conditions labeled as "specifically coupled" also had 20 mM EDC as the coupling reagent, while "nonspecifically bound" conditions were carried out in the absence of EDC. As a first test, we coupled an Os-based redox reporter that was previously reported by Pellitero and colleagues.[35] While we coupled it to many polymers, Figure 6A specifically shows the Os reporter on films of DHTDC formed at 1.35 V for 20 s in acetonitrile with TBATFB as an example. The Os reporter has a redox potential around +0.2 V, enabling interrogation in the positive direction (Figure 6A). Because of these positive potentials, we avoided reduction and loss of the conductivity of the underlying DHTDC film. However, while we demonstrated successful

https://doi.org/10.1021/acsapm.3c02206
ACS Appl. Polym. Mater. 2024, 6, 541−551

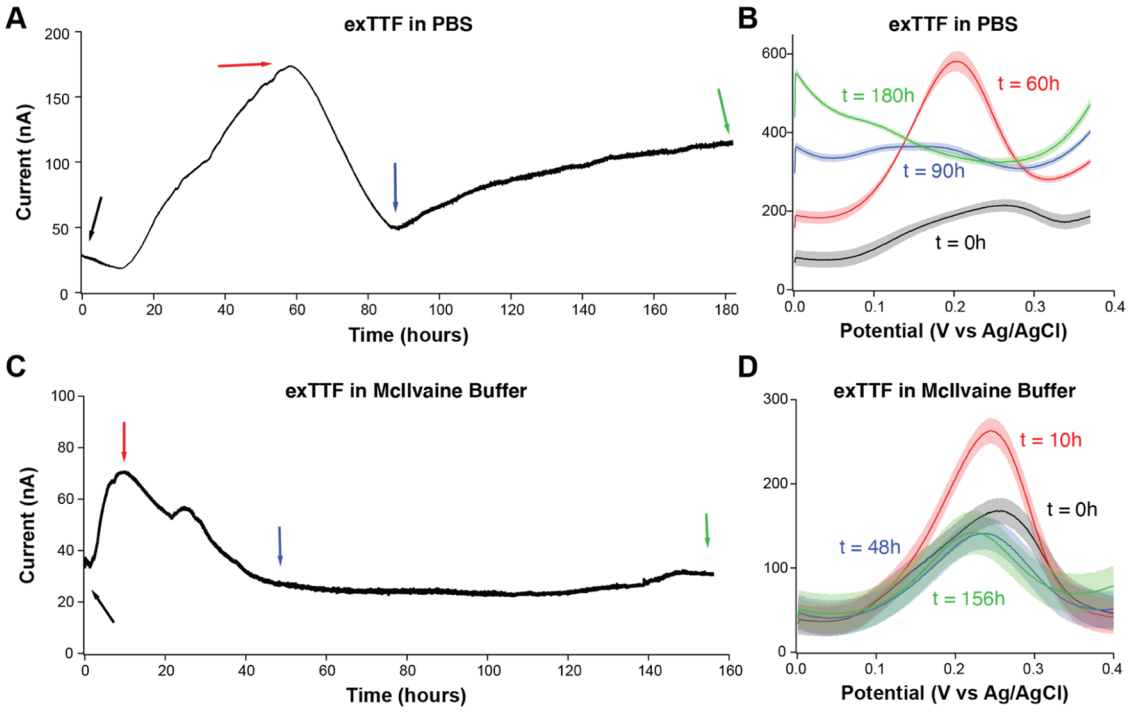

Figure 7. Signal stability of exTTF on gold electrodes. By repeatedly interrogating exTTF-functionalized Au electrodes by SWV (25 mV, 60 Hz) every 10 s for a week, we demonstrate that (A) in PBS, current increases over the first 60 h and then rapidly decays below the point of peak resolution. (B) Voltammograms show that after 80 h of continuous interrogation, the voltammogram baseline increases, causing the current increase observed in panel (A). (C) In chloride-free McIlvaine buffer, the current again increases over the first 10 h, then slowly equilibrates to a stable current magnitude. Panels (B, D) are extracted voltammograms from the color-matched times marked in panels (A, C), respectively. Solid lines are the mean, and shaded areas represent the standard deviation calculated from 8 electrodes.

SWV (25 mV, 2500 Hz) signaling with this reporter, there was no discernible difference between specifically coupled and nonspecifically bound peaks. This inability to differentiate occurs due to the "sticky" nature of the Os complex, which causes it to resist desorption from the polymer surface, even upon washing with 6 M guanidine hydrochloride and acetonitrile.

We next tested aminoferrocene (AmFc), which has a redox potential around +0.15 V. While we successfully coupled this reporter to many polymers, Figure 6B specifically shows AmFc on films of DHTDC formed at 1.1 V for 60 min in acetonitrile with TBATFB as an example. Here, we demonstrate successful SWV (25 mV, 60 Hz) signaling with the reporter, including a discernible difference between specifically coupled from nonspecifically bound (Figure 6B). Unfortunately, AmFc is known to be labile in chloride-containing media.[36] Since we are most interested in deploying sensors in biologically relevant environments that contain high concentrations of chloride, we did not pursue stability evaluations or further analytical validations with this reporter. However, the successful demonstration of reporter coupling with minimal nonspecific binding offers promise toward the discovery of a more suitable redox reporter for interfacing with these conductive polymers.

The final reporter we tested was a π-extended tetrathiafulvalene molecule (exTTF) previously reported by Li and colleagues for the fabrication of pH-independent electrochemical aptamer-based sensors.[37] Because this molecule has a free carboxylic acid instead of an amine, we first had to change the thiophene monomer we were using for polymer formation to enable EDC coupling. Here, we polymerized either 2-(thiophen-3-yl)ethan-1-amine (TEA) or 2-(3-methyl-2-thienyl) ethanamine (MTEA) by holding at 1.4 V for 60 min in acetonitrile with TBATFB. After coupling exTTF and interrogating via SWV (25 mV, 250 Hz), we revealed a strong faradic peak around +0.35 V for the specifically coupled condition only (Figure 6C). While Figure 6C displays the SWVs for MTEA interrogation in PBS, similar graphs are obtained for TEA as well as interrogation in the buffer (McIlvaine) originally reported by Li and colleagues.[37] We are unsure why this redox potential does not match the near 0 V that was previously reported, but we believe it may be that coupling the reporter to DNA (as previously reported) versus directly to the polymer may change its electronic properties. In support of this hypothesis, by interrogating solution-phase exTTF (100 μM) rather than polymer-coupled reporter, the oxidation peak is shifted lower, occurring around +0.15 V (Figure S4). Additionally, previous reports have shown changes in the peak potential for exTTF oxidation based on temperature and pH,[38−40] so these factors could be contributing to the shift as well. Regardless of the shift in redox potential, the clear difference between specifically coupled and nonspecifically bound peaks proved promising for use of exTTF with thiophene polymers. To investigate further, we repeatedly interrogated the electrodes and found that the faradic peak disappeared within five SWV scans (Figure 6C, blue trace). We currently do not know if this extremely rapid signal loss is due to degradation of the reporter, polymer, or some combination of factors, but this will be an area for future study.

Motivated by the initial results observed with exTTF on conductive polymers, we sought to study this redox reporter on more traditional thiol-on-gold monolayers. Here, we modified Au disk electrodes with mixed SAMs via overnight incubation in 100 μM 8-aminooctanethiol (AmOcSH) and 1 mM 6-

https://doi.org/10.1021/acsapm.3c02206
ACS Appl. Polym. Mater. 2024, 6, 541−551

Table 2. Polymer/Redox Reporter Combinations and Observations

polymer	redox reporter	buffer	observations
poly(*m*-PD)	MB-ester	PBS	too thick and dense for electron transfer (ET) to MB or DNA
poly(*p*/*o*-PD)	MB-ester/carboxy-DNA	PBS	thick. Too dense for ET to DNA but not to MB
PPA/TBA/DHTDC	NMB	PBS	loss of conductivity when scanning negative
DHTDC	AmFc	PBS	good coupling but unstable in chloride media
DHTDC	Os	PBS	nonspecific binding
MTEA	exTTF	PBS/McIlvaine	good coupling but unexplained, rapid signal loss
TEA	exTTF	PBS/McIlvaine	good coupling but unexplained, rapid signal loss

mercapto-hexanol (MCH) in 50% ethanol. We then coupled exTTF and interrogated the resulting surfaces via SWV (25 mV, 60 Hz) in either PBS or McIlvaine buffer, both at pH ∼ 7.4. In our hands, monolayer-coupled exTTF underwent oxidation at around +0.25 V in McIlvaine buffer (Figure S5). Considered together with our exTTF results on Pt (Figures 6 and S4), we still believe that coupling the reporter to DNA versus directly to the monolayer or polymer may be the reason for the discrepancy in the reduction potential. Future work will aim to couple this reporter to thiolated DNA prior to surface deposition. Additionally, slight differences in experimental parameters may be responsible for the shift.[38−40] However, despite the shift in redox potential, we still observed a marked difference in the specifically coupled vs nonspecifically bound exTTF (Figure S5), so we further evaluated the signaling stability of the reporter on these surfaces. By serially interrogating monolayer-coated gold electrodes every 10 s for a week (Figure 7), we found that after an initial increase in signal, these electrodes displayed different behavior based on the buffer system employed. Specifically, in PBS, the current reaches a maximum at around 60 h and then rapidly decays beyond the point of peak resolution (Figure 7A,B). On the other hand, when interrogated in McIlvaine buffer, the current reaches a maximum within 10 h and then slowly equilibrates to a stable current for the entire week (Figure 7C,D).

We are unsure why the current in both cases initially increases, as we have not observed this with other redox reporters. However, we speculate it may be due to the stabilization of different radical species. Tetrathiafulvalenes are known to form radical cations or even dications that could be stabilized by anions in solution.[41] exTTF, specifically, is known to undergo structural reorganization when forming the dicationic species,[40] which is likely further contributing to the initial signal change. Beyond the initial increase in current, it appears that the signal stability of these thiol/exTTF-modified electrodes may be modulated by the presence of chloride in solution. While in PBS the baseline current increases over time (Figure 7B), in McIlvaine buffer, the baseline current remains constant over the entire interrogation period (Figure 7D). It is possible that scanning so far positive could be oxidizing the underlying gold, which can then form soluble gold chloride in PBS and promote dissolution of the thiol monolayers.[42] With this in mind and supported by the ability to resolve faradaic peak after 156 h of continuous interrogation in McIlvaine buffer, we believe the exTTF reporter itself is not degrading. Rather, signal loss is caused by thiol monolayer degradation (as with Au electrodes in PBS) or some interaction between exTTF and MTEA or Pt (as in Figure 6C). Still, exTTF shows great promise for extending the operational lifetime of NBE sensors. Significant efforts will be devoted in the future to altering its reduction potential closer to 0 V and determining the mechanism of signal loss when coupled to conductive polymers.

CONCLUSIONS

In this work, we explored the formation and modification of conductive polymers on Pt electrodes for the fabrication of NBE sensors. Specifically, we investigated polymers of aromatic amines, pyrroles, and thiophenes. For each tested molecule, we first determined the extent to which the deposited polymer covered the electrode surface via the passivation of the ORR in dilute sulfuric acid. These results, along with the solvent, counterion, electrochemical method, and parameters used for polymerization, are summarized in Table 1.

Following polymer formation, we coupled redox reporters or reporter-modified nucleic acids to the surface via EDC coupling reactions. The specific combinations of the polymer and redox reporter are summarized in Table 2, alongside our observations for each. For polymers of PD, extensive modification of monomer concentrations, CV scan rate, number of CV cycles, and counterions used during polymerization did not enable signaling with reporter-modified nucleic acids. Notably, we believe polymers formed from PD are too thick to allow electron transfer between the surface of the electrode and the surface of the polymer. While poly(*o*-PD) and poly(*p*-PD) films allow signaling with MB, we believe this is enabled by MB-ester diffusing into the pores of the polymer, whereas much larger nucleic acids are restricted to the polymer surface. This argument is supported by the known balance between thickness and charge carrier permeability for polymers of aromatic amines.[28] However, it may still be possible to disrupt the polymer structure enough to enable signaling with reporter-modified nucleic acids. Future attempts could include a bulky, disruptive copolymer to introduce holes large enough for nucleic acid penetration into the polymer. They could also try further tuning electropolymerization conditions to densify polymeric films on the electrode surface. For example, using a high voltage, pulsed voltammetric technique could produce less uniform PD polymers that enable electron transfer to the electrode surface.

In terms of pyrrole and thiophene polymers, interrogation at the negative potentials needed for MB reduction causes a change in the conductivity and electron transfer capabilities of the films. To overcome this inherent limitation, we coupled several reporters with positive redox potentials and demonstrated successful electron transfer. Unfortunately, no combination of polymer/reporter has yet produced a surface with both stable signal under continuous voltammetric interrogation and low nonspecific binding. However, we are optimistic that such a combination exists. It is possible that coupling the Os[35] or exTTF[37] reporters to nucleic acids prior to surface exposure could reduce the levels of nonspecific binding or change the

https://doi.org/10.1021/acsapm.3c02206
ACS Appl. Polym. Mater. 2024, 6, 541−551

electronic properties, respectively. Additionally, different reporters with positive redox potentials may interface with Pt electrodes and thiophene polymers more favorably. As such, all of these options could be explored in future work. This study provides a starting framework for future exploration of conductive polymer chemistries and redox reporters with the goal of developing NBE sensors with materials relevant to biomedical applications.

MATERIALS AND METHODS

Chemicals and Materials. 6-mercapto-1-hexanol (MCH, Cat. #451088), 1*H*-pyrrole-1-propionic acid (PPA, Cat. #687545), 2-(3-methyl-2-thienyl)ethanamine hydrochloride (MTEA, Cat. #CBR01050), sodium 4-vinylbenzenesulfonate (VBS, Cat. #94904), *para*-phenylenediamine (*p*-PD, Cat. #P6001), *meta*-phenylenediamine (*m*-PD, Cat. #P23954), sodium sulfate (Cat. #239313), sodium phosphate dibasic (Cat. #S3264), citric acid (Cat. #251275), aminoferrocene (AmFc, Cat. #07379), 8-amino-1-octanethiol hydrochloride (AmOcSH, Cat. #745774), and *N*-(3-(dimethylamino)-propyl)-*N*′-ethylcarbodiimide hydrochloride (EDC, Cat. #E7750) were purchased from Sigma-Aldrich (St. Louis, MO). Phosphate-buffered saline (PBS, 11.9 mM HPO32-; 137 mM NaCl; 2.7 mM KCl; pH = 7.4, Cat. #BP399), sulfuric acid (H_2SO_4 Cat. #A510), sodium hydroxide (NaOH, Cat. #S318), magnesium chloride hexahydrate ($MgCl_2$ Cat. #BP214), and sodium chloride (NaCl, Cat. #S271) were purchased from Fisher Scientific (Waltham, MA). Ethanol (catalog No. 111000200) was purchased from Pharmco (Brookfield, CT). New methylene blue zinc chloride double salt (NMB, cat. No. 192020100) and guanidine hydrochloride (cat. No. 120230010) were purchased from Acros Organics (Fair Lawn, NJ). *ortho*-Phenylenediamine (*o*-PD, cat. No. 34005) was purchased from Thermo Scientific (Rockford, IL). 2-(thiophen-3-yl)ethan-1-amine (TEA, catalog No. AB522300) was purchased from abcr (Karlsruhe, Germany). 2,3-dihydrothieno[3,4-B][1,4]dioxine-2-carboxylic acid (DHTDC, Cat. #A10769) was purchased from AstaTech (Bristol, PA). Tetrabutylammonium tetrafluoroborate (TBATFB, cat. No. T0914) was purchased from Tokyo Chemical Industry (Portland, OR). 4-(3-Thienyl)butyric acid (TBA, catalog No. 4134) was purchased from Rieke Metals (Lincoln, NE). Methylene blue succinimidyl ester (MB-ester, catalog No. 40075) was purchased from Biotium (Fremont, CA). The exTTF reporter was synthesized by the original authors of ref 37 and kindly donated to our group. The Os reporter was synthesized following protocols found in ref. 35

We prepared all aqueous solutions using deionized water from a Milli-Q Direct purification system, with a resistivity of 18 MΩ. Coupling buffer contained 250 mM NaCl and 5 mM $MgCl_2$. McIlvaine buffer (pH ∼ 7.4) contained 1.75 g of L^{-1} citric acid and 25.75 g of L^{-1} dibasic sodium phosphate. All electrochemical experiments were performed in 1× PBS.

Platinum working electrodes consisted of smooth ring electrode arrays (see, for example, Figure S2, 8 electrodes per array), with each electrode element having an internal diameter of 50 μm and an external diameter of 100 μm, manufactured by Biolinq (San Diego, CA). The arrays had an average variability in surface area of ±10% across all devices and a roughness factor of 1.1 relative to their geometrical area. Each electrode array was used only once per experiment and then discarded. Gold working electrodes (Cat. #002314, diameter: 1.6 mm) were obtained from ALS Inc. (Tokyo, Japan). Platinum wire counter electrodes (Cat. #CH115) and Ag/AgCl reference electrodes (Cat. #CHI111) were purchased from CH Instruments (Austin, TX). For polishing gold electrodes, cloth pads (Cat. #MF-1040) and alumina slurry (Cat. #CF-1050) were purchased from BASi (West Lafayette, IN).

Oligonucleotides were purchased from IDT (Table 3). Carboxyl-modified oligonucleotides contained proprietary modifications for the free carboxyl and methylene blue on the 5′ and 3′ ends, respectively. The modifications for amine-terminated oligonucleotides had the following structures:

Amine modification at the 5′ terminus:

Table 3. DNA Sequence Employed in This Work

target	sequence	ref
aminoglycoside	5′-GGG ACT TGG TTT AGG TAA TGA GTC CC-3′	43

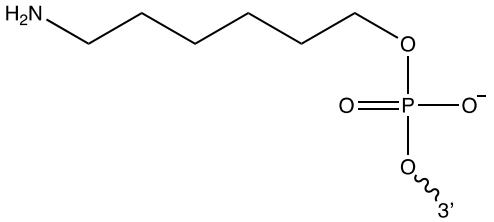

Methylene blue (MB) modification at the 3′ terminus:

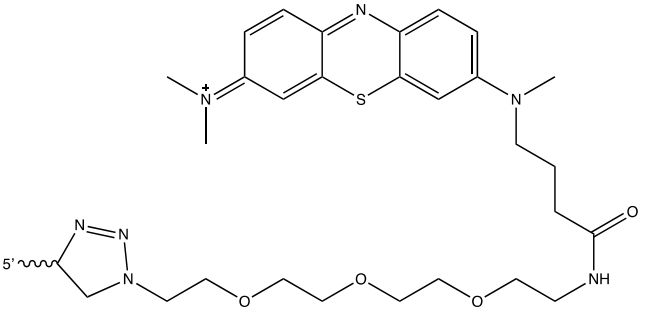

Gold Electrode Preparation. Gold electrodes were polished for ∼3 min on a cloth pad with alumina slurry. After sonicating (Branson 2800) in ethanol to remove polishing debris, they were then electrochemically cleaned in 0.5 M NaOH and 0.5 M H_2SO_4 following a previously reported protocol.[44] Briefly, (1) in 0.5 M NaOH, we scanned from −0.3 to −1.6 V vs AglAgCl, 200 times at a scan rate of 0.5 V/s; (2) in 0.5 M H_2SO_4, we scanned from 0 to 1.6 V vs AglAgCl, 200 times at a scan rate of 0.5 V/s. Once the electrodes showed reproducible voltammograms in sulfuric acid, we rinsed them with water, placed them immediately into a solution of 1 mM MCH and 100 μM AmOcSH, and then left them to incubate overnight. After monolayer formation, electrodes were incubated overnight in 100 μM solutions of exTTF in a coupling buffer with 20 mM EDC. Fully fabricated sensors were then placed in a cell with 1× PBS for electrochemical measurements.

Conductive Polymer Preparation. Platinum electrodes were cleaned by CV cycling in 0.5 M sulfuric acid in *a* two-step procedure: (1) 200 cycles between −0.25 and +1.25 V at a scan rate of 500 mV s^{-1}; (2) 30 cycles between −0.23 and +1.24 V at a scan rate of 10 mV/s. Once reproducible hydrogen adsorption/desorption peaks were obtained in the voltammograms, electrodes were immediately placed in 50 mM sulfuric acid for passivation determination. Following CV measurement in 50 mM sulfuric acid, polymers were electrochemically formed on electrodes according to the following respective method:

- Aromatic amines: CV cycling (0 to 1 V; 5, 10, 25, 50, or 100 mV s^{-1}) in monomer solution (5, 10, 25, 50, or 100 mM) in PBS with 5 mM sodium sulfate.
- Pyrroles: 30 pulse repetitions of (1) 1 V for 1 s; (2) 0 V for 10 s in 50 mM monomer solutions in saline.
- Thiophenes: Holding electrode potential for either 20 s or 60 min in 10 mM monomer solutions.
  - 1.4 V for MTEA in acetonitrile with 100 mM TBATFB.
  - 1.35 or 1.1 V for TBA or DHTDC in acetonitrile with 100 mM TBATFB.
  - 0.9 V for TBA or DHTDC in water with 100 mM VBS.

After polymer deposition, modified electrodes were exposed to redox reporter (100 μM) or DNA (1 μM) solutions in coupling buffer ±20 mM EDC overnight. DNA concentration was determined via molecular absorbance measurements employing an Implen Nano-

https://doi.org/10.1021/acsapm.3c02206
ACS Appl. Polym. Mater. 2024, 6, 541−551

photometer NP80. Fully functionalized electrodes were thoroughly washed with PBS and then interrogated electrochemically.

Electrochemical Measurements. A CH Instruments electrochemical analyzer (CHI 1040C, Austin, TX) multichannel potentiostat and associated software were used for all CV and SWV measurements. We used a three-electrode cell configuration consisting of platinum working, platinum wire counter, and AglAgCl (saturated KCl) reference electrodes. Cyclic voltammetry measurements for determination of % passivation were recorded at a scan rate of 1 V s^{-1} in the potential window 0 to −0.45 V vs AglAgCl. Current was sampled every millisecond. SWV measurements were performed with a square-wave amplitude of 25 mV, step size of 1 mV, and various frequencies.

Data Analysis. We employed a previously reported, open-source Python script called SACMES[45] for the processing of our electrochemical measurements. Graphs were created in Igor Pro v8.

■ ASSOCIATED CONTENT

Supporting Information

The Supporting Information is available free of charge at https://pubs.acs.org/doi/10.1021/acsapm.3c02206.

Optimization of poly(PD) deposition conditions (Figure S1); PD polymer thickness measurements (Figure S2); effect of voltage and counterions during DHTDC deposition (Figure S3); voltammogram of solution-phase exTTF (Figure S4), and voltammograms of surface-coupled exTTF (Figure S5) (PDF)

■ AUTHOR INFORMATION

Corresponding Author

Netzahualcóyotl Arroyo-Currás − *Department of Pharmacology and Molecular Sciences, Johns Hopkins University School of Medicine, Baltimore, Maryland 21202, United States; Department of Chemical and Biomolecular Engineering and Institute for NanoBioTechnology, Whiting School of Engineering, Johns Hopkins University, Baltimore, Maryland 21218, United States;* Present Address: 316 Hunterian Building, Johns Hopkins University School of Medicine, 725 North Wolfe Street, Baltimore, Maryland 21205, United States; Phone: 443-287-4798; Email: netzarroyo@jhmi.edu

Authors

Alexander Shaver − *Department of Pharmacology and Molecular Sciences, Johns Hopkins University School of Medicine, Baltimore, Maryland 21202, United States;* orcid.org/0000-0002-5478-5291

Kyle Mallires − *Biolinq Inc., San Diego, California 92121, United States*

Jonathan Harris − *Biolinq Inc., San Diego, California 92121, United States*

Jonathan Kavner − *Biolinq Inc., San Diego, California 92121, United States*

Bo Wang − *Biolinq Inc., San Diego, California 92121, United States*

Rebecca Gottlieb − *Biolinq Inc., San Diego, California 92121, United States*

Juan Lión-Villar − *Department of Organic Chemistry, Faculty of Chemistry, Universidad Complutense de Madrid, 28040 Madrid, Spain;* orcid.org/0009-0008-9883-0104

María Ángeles Herranz − *Department of Organic Chemistry, Faculty of Chemistry, Universidad Complutense de Madrid, 28040 Madrid, Spain*

Nazario Martín − *Department of Organic Chemistry, Faculty of Chemistry, Universidad Complutense de Madrid, 28040 Madrid, Spain; IMDEA-Nanociencia, 28049 Madrid, Spain*

Complete contact information is available at: https://pubs.acs.org/10.1021/acsapm.3c02206

Author Contributions

A.S. and N.A.C. developed the idea. J.L.-V., M.A.H., and N.M. synthesized exTTF. A.S. performed all electrochemical experiments. K.M., J.H., J.K., B.W., and R.G. provided intellectual input. All authors participated in the writing and editing of this manuscript.

Funding

This work was supported by SEMI through the Nano-Bio Materials Consortium under Project NB18−21−30. The content is solely the responsibility of the authors.

Notes

The authors declare the following competing financial interest(s): K.M., J.H., J.K., B.W., and R.G. are employees of Bioling Inc., a company pursuing the commercialization of nucleic acid-based electrochemical sensors.

■ ACKNOWLEDGMENTS

J.L.-V., M.A.H., and N. M. acknowledge financial support by the Spanish Ministry of Science and Innovation (MICIN) through projects PID2020-114653RB-I00 and PID2020-115120GB-I00 v.

■ REFERENCES

(1) Hommel, E.; Olsen, B.; Battelino, T.; Conget, I.; Schutz-Fuhrmann, I.; Hoogma, R.; Schierloh, U.; Sulli, N.; Gough, H.; Castaneda, J.; de Portu, S.; Bolinder, J. Impact of continuous glucose monitoring on quality of life, treatment satisfaction, and use of medical care resources: analyses from the SWITCH study. *Acta Diabetol.* **2014**, *51*, 845−851.

(2) Qu, L.; Xu, J.; Tan, X.; Liu, Z.; Xu, L.; Peng, R. Dual-aptamer modification generates a unique interface for highly sensitive and specific electrochemical detection of tumor cells. *ACS Appl. Mater. Interfaces* **2014**, *6*, 7309−7315.

(3) Xiao, Y.; Lubin, A. A.; Heeger, A. J.; Plaxco, K. W. Label-free electronic detection of thrombin in blood serum by using an aptamer-based sensor. *Angew. Chem., Int. Ed.* **2005**, *44*, 5456−5459.

(4) Campbell, A. S.; Kim, J.; Wang, J. Wearable Electrochemical Alcohol Biosensors. *Curr. Opin. Electrochem.* **2018**, *10*, 126−135.

(5) Arroyo-Currás, N.; Ortega, G.; Copp, D. A.; Ploense, K. L.; Plaxco, Z. A.; Kippin, T. E.; Hespanha, J. P.; Plaxco, K. W. High-Precision Control of Plasma Drug Levels Using Feedback-Controlled Dosing. *ACS Pharmacol. Transl. Sci.* **2018**, *1*, 110−118.

(6) Dauphin-Ducharme, P.; Yang, K.; Arroyo-Curras, N.; Ploense, K. L.; Zhang, Y.; Gerson, J.; Kurnik, M.; Kippin, T. E.; Stojanovic, M. N.; Plaxco, K. W. Electrochemical Aptamer-Based Sensors for Improved Therapeutic Drug Monitoring and High-Precision, Feedback-Controlled Drug Delivery. *ACS Sens.* **2019**, *4*, 2832−2837.

(7) Singh, A. K.; Mittal, S.; Das, M.; Saharia, A.; Tiwari, M. Optical biosensors: a decade in review. *Alexandria Eng. J.* **2023**, *67*, 673−691.

(8) Stanciu, L. A.; Wei, Q.; Barui, A. K.; Mohammad, N. Recent Advances in Aptamer-Based Biosensors for Global Health Applications. *Annu. Rev. Biomed. Eng.* **2021**, *23*, 433−459.

(9) Baker, B. R.; Lai, R. Y.; Wood, M. S.; Doctor, E. H.; Heeger, A. J.; Plaxco, K. W. An electronic, aptamer-based small-molecule sensor for the rapid, label-free detection of cocaine in adulterated samples and biological fluids. *J. Am. Chem. Soc.* **2006**, *128*, 3138−3139.

(10) Li, H.; Dauphin-Ducharme, P.; Ortega, G.; Plaxco, K. W. Calibration-Free Electrochemical Biosensors Supporting Accurate

Molecular Measurements Directly in Undiluted Whole Blood. *J. Am. Chem. Soc.* **2017**, *139*, 11207−11213.
(11) Macovei, D. G.; Irimes, M. B.; Hosu, O.; Cristea, C.; Tertis, M. Point-of-care electrochemical testing of biomarkers involved in inflammatory and inflammatory-associated medical conditions. *Anal. Bioanal. Chem.* **2023**, *415*, 1033−1063.
(12) Huang, Y.; Zhang, L.; Ji, Y.; Deng, H.; Long, M.; Ge, S.; Su, Y.; Chan, S. Y.; Loh, X. J.; Zhuang, A.; Ruan, J. A non-invasive smart scaffold for bone repair and monitoring. *Bioact. Mater.* **2023**, *19*, 499−510.
(13) Xue, T.; Attarilar, S.; Liu, S.; Liu, J.; Song, X.; Li, L.; Zhao, B.; Tang, Y. Surface Modification Techniques of Titanium and its Alloys to Functionally Optimize Their Biomedical Properties: Thematic Review. *Front. Bioeng. Biotechnol.* **2020**, *8*, No. 603072.
(14) Zhou, L.; Beuerman, R. W. Tear analysis in ocular surface diseases. *Prog. Retinal Eye Res.* **2012**, *31*, 527−550.
(15) Xiao, Y.; Lai, R. Y.; Plaxco, K. W. Preparation of electrode-immobilized, redox-modified oligonucleotides for electrochemical DNA and aptamer-based sensing. *Nat. Protoc.* **2007**, *2*, 2875−2880.
(16) Pellitero, M. A.; Shaver, A.; Arroyo-Currás, N. Critical Review—Approaches for the Electrochemical Interrogation of DNA-Based Sensors: A Critical Review. *J. Electrochem. Soc.* **2020**, *167*, No. 037529.
(17) Arroyo-Currás, N.; Somerson, J.; Vieira, P. A.; Ploense, K. L.; Kippin, T. E.; Plaxco, K. W. Real-time measurement of small molecules directly in awake, ambulatory animals. *Proc. Natl. Acad. Sci. U.S.A.* **2017**, *114*, 645−650.
(18) Shaver, A.; Mahlum, J. D.; Scida, K.; Johnston, M. L.; Aller Pellitero, M.; Wu, Y.; Carr, G. V.; Arroyo-Curras, N. Optimization of Vancomycin Aptamer Sequence Length Increases the Sensitivity of Electrochemical, Aptamer-Based Sensors In Vivo. *ACS Sens.* **2022**, *7*, 3895−3905.
(19) Wu, Y.; Tehrani, F.; Teymourian, H.; Mack, J.; Shaver, A.; Reynoso, M.; Kavner, J.; Huang, N.; Furmidge, A.; Duvvuri, A.; Nie, Y.; Laffel, L. M.; Doyle, F. J., 3rd; Patti, M. E.; Dassau, E.; Wang, J.; Arroyo-Curras, N. Microneedle Aptamer-Based Sensors for Continuous, Real-Time Therapeutic Drug Monitoring. *Anal. Chem.* **2022**, *94*, 8335−8345.
(20) Lin, S.; Cheng, X.; Zhu, J.; Wang, B.; Jelinek, D.; Zhao, Y.; Wu, T. Y.; Horrillo, A.; Tan, J.; Yeung, J.; Yan, W.; Forman, S.; Coller, H. A.; Milla, C.; Emaminejad, S. Wearable microneedle-based electrochemical aptamer biosensing for precision dosing of drugs with narrow therapeutic windows. *Sci. Adv.* **2022**, *8*, No. eabq4539.
(21) Clark, V.; Pellitero, M. A.; Arroyo-Curras, N. Explaining the Decay of Nucleic Acid-Based Sensors under Continuous Voltammetric Interrogation. *Anal. Chem.* **2023**, *95*, 4974−4983.
(22) Shaver, A.; Curtis, S. D.; Arroyo-Curras, N. Alkanethiol Monolayer End Groups Affect the Long-Term Operational Stability and Signaling of Electrochemical, Aptamer-Based Sensors in Biological Fluids. *ACS Appl. Mater. Interfaces* **2020**, *12*, 11214−11223.
(23) Leung, K. K.; Downs, A. M.; Ortega, G.; Kurnik, M.; Plaxco, K. W. Elucidating the Mechanisms Underlying the Signal Drift of Electrochemical Aptamer-Based Sensors in Whole Blood. *ACS Sens.* **2021**, *6*, 3340−3347.
(24) Guo, B.; Ma, P. X. Conducting Polymers for Tissue Engineering. *Biomacromolecules* **2018**, *19*, 1764−1782.
(25) Nezakati, T.; Seifalian, A.; Tan, A.; Seifalian, A. M. Conductive Polymers: Opportunities and Challenges in Biomedical Applications. *Chem. Rev.* **2018**, *118*, 6766−6843.
(26) Balint, R.; Cassidy, N. J.; Cartmell, S. H. Conductive polymers: towards a smart biomaterial for tissue engineering. *Acta Biomater.* **2014**, *10*, 2341−2353.
(27) Losito, I.; Palmisano, F.; Zambonin, P. G. o-Phenylenediamine Electropolymerization by Cyclic Voltammetry Combined with Electrospray Ionization-Ion Trap Mass Spectrometry. *Anal. Chem.* **2003**, *75*, 4988−4995.
(28) Budnikov, H. C.; Evtugyn, G. A.; Porfireva, A. V. Electrochemical DNA sensors based on electropolymerized materials. *Talanta* **2012**, *102*, 137−155.
(29) Shaver, A.; Arroyo-Curras, N. The challenge of long-term stability for nucleic acid-based electrochemical sensors. *Curr. Opin. Electrochem.* **2022**, *32*, No. 100902.
(30) Peng, H.; Zhang, L.; Soeller, C.; Travas-Sejdic, J. Conducting polymers for electrochemical DNA sensing. *Biomaterials* **2009**, *30*, 2132−2148.
(31) Zhang, X.; Tan, X.; Wang, P.; Qin, J. Application of Polypyrrole-Based Electrochemical Biosensor for the Early Diagnosis of Colorectal Cancer. *Nanomaterials* **2023**, *13*, No. 674.
(32) Jenkins, J.; Ratcliff, E.; Shallcross, R. C.; Head, J.; Armstrong, N. In *Photovoltaic Devices Created from Electrodeposited Nano-Textured Poly(thiophene) Films*, SPIE Proceedings; SPIE, 2008.
(33) Bufon, C. C. B.; Heinzel, T.; Espindola, P.; Heinze, J. Influence of the polymerization potential on the transport properties of polypyrrole films. *J. Phys. Chem. B* **2010**, *114*, 714−718.
(34) Ramanavicius, A.; Oztekin, Y.; Ramanaviciene, A. Electrochemical formation of polypyrrole-based layer for immunosensor design. *Sens. Actuators, B* **2014**, *197*, 237−243.
(35) Aller Pellitero, M.; Kundu, N.; Sczepanski, J.; Arroyo-Curras, N. Os(II/III) complex supports pH-insensitive electrochemical DNA-based sensing with superior operational stability than the benchmark methylene blue reporter. *Analyst* **2023**, *148*, 806−813.
(36) Kang, D.; Ricci, F.; White, R. J.; Plaxco, K. W. Survey of Redox-Active Moieties for Application in Multiplexed Electrochemical Biosensors. *Anal. Chem.* **2016**, *88*, 10452−10458.
(37) Li, S.; Ferrer-Ruiz, A.; Dai, J.; Ramos-Soriano, J.; Du, X.; Zhu, M.; Zhang, W.; Wang, Y.; Herranz, M. A.; Jing, L.; Zhang, Z.; Li, H.; Xia, F.; Martin, N. A pH-independent electrochemical aptamer-based biosensor supports quantitative, real-time measurement in vivo. *Chem. Sci.* **2022**, *13*, 8813−8820.
(38) Liu, S. G.; Perez, I. I.; Martin, N.; Echegoyen, L. Intramolecular electronic interactions in conjugated ferrocene-pi-extended-tetrathiafulvalene donor-pi-donor molecular hybrids. *J. Org. Chem.* **2000**, *65*, 9092−9102.
(39) Pérez, I.; Liu, S. G.; Martin, N.; Echegoyen, L. Synthesis and properties of conjugated hybrid tetrathiafulvalene dimers. *J. Org. Chem.* **2000**, *65*, 3796−3803.
(40) Herranz, M. A.; Yu, L.; Martin, N.; Echegoyen, L. Synthesis, electrochemistry and self-assembled monolayers of novel tetrathiafulvalene (TTF) and pi-extended TTF (exTTF) disulfides. *J. Org. Chem.* **2003**, *68*, 8379−8385.
(41) Gao, F.; Zhu, F. F.; Wang, X. Y.; Xu, Y.; Wang, X. P.; Zuo, J. L. Stabilizing radical cation and dication of a tetrathiafulvalene derivative by a weakly coordinating anion. *Inorg. Chem.* **2014**, *53*, 5321−5327.
(42) Korolev, I.; Spathariotis, S.; Yliniemi, K.; Wilson, B. P.; Abbott, A. P.; Lundström, M. Mechanism of selective gold extraction from multi-metal chloride solutions by electrodeposition-redox replacement. *Green Chem.* **2020**, *22*, 3615−3625.
(43) Schoukroun-Barnes, L. R.; Wagan, S.; White, R. J. Enhancing the analytical performance of electrochemical RNA aptamer-based sensors for sensitive detection of aminoglycoside antibiotics. *Anal. Chem.* **2014**, *86*, 1131−1137.
(44) Arroyo-Currás, N.; Scida, K.; Ploense, K. L.; Kippin, T. E.; Plaxco, K. W. High Surface Area Electrodes Generated via Electrochemical Roughening Improve the Signaling of Electrochemical Aptamer-Based Biosensors. *Anal. Chem.* **2017**, *89*, 12185−12191.
(45) Curtis, S. D.; Ploense, K. L.; Kurnik, M.; Ortega, G.; Parolo, C.; Kippin, T. E.; Plaxco, K. W.; Arroyo-Curras, N. Open Source Software for the Real-Time Control, Processing, and Visualization of High-Volume Electrochemical Data. *Anal. Chem.* **2019**, *91*, 12321−12328.

https://doi.org/10.1021/acsapm.3c02206
ACS Appl. Polym. Mater. 2024, 6, 541−551